Fluoroimmunoassay of influenza virus using sulfur-doped graphitic carbon nitride quantum dots coupled with Ag2S nanocrystals

Fluoroimmunoassay of influenza virus using sulfur doped-graphitic carbon nitride quantum dots coupled with Ag_2S nanocrystals

Ojodomo J. Achadu[a], De Xing Lioe[b], Keiichiro Kagawa[b], Shoji Kawahito[b], Enoch Y. Park[a,c,*]

[a] *Research Institute of Green Science and Technology, Shizuoka University, 836 Ohya Suruga-ku, Shizuoka 422-8529, Japan*

[b] *Research Institute of Electronics, Shizuoka University, 3-5-1 Johoku, Nakaku, Hamamatsu, Shizuoka 432-8011, Japan*

[c] *Laboratory of Biotechnology, Department of Bioscience, Graduate School of Science and Technology, Shizuoka University, 836 Ohya Suruga-ku, Shizuoka 422-8529, Japan*E-mail:

ojodomo.john.achadu@shizuoka.ac.jp (OJA) (ORCID: 0000-0002-5542-3110)

lioe@idl.rie.shizuoka.ac.jp (DXL)

kagawa@idl.rie.shizuoka.ac.jp (KK)

kawahito@idl.rie.shizuoka.ac.jp (SK)

park.enoch@shizuoka.ac.jp (EYP) (0000-0002-7840-1424)

[*] Corresponding author: Research Institute of Green Science and Technology, Shizuoka University, 836 Ohya, Suruga-ku, Shizuoka 422-8529, Japan.
E-mail address: park.enoch@shizuoka.ac.jp (E.Y. Park). Tel (Fax): +81-54-238-4887

Abstract

A novel sulfur-doped graphitic carbon nitride quantum dots (S-gCNQDs) are synthesized using a single-source precursor in a one-step solvothermal process. The S-gCNQDs with a size of ~5 nm display a strong green intrinsic fluorescence at 512 nm when excited at 400 nm, with a quantum yield of ~ 33 % in aqueous solution. The prepared S-gCNQDs and Ag_2S nanocrystals were applied as innovative functional materials to fabricate a biosensor for virus detection based on the conjugation of specific anti-human influenza A monoclonal antibody to the S-gCNQDs and Ag2S NCs, respectively. In the presence of the influenza A virus, an interaction between the S-gCNQDs/Ag2S-labeled antibody resulted in the formation of a nanosandwich structure, which is accompanied by the fluorescence enhancement of the S-gCNQDs. The change in fluorescence intensity is linearly correlated with the concentration of the influenza A virus (H1N1) in the 10 fg/mL to 1.0 ng/mL range, with a limit of detection of 5.5 fg/mL. The assay was further applied to the determination of clinically isolated influenza A virus (H3N2/Yokohama) mixed with human serum. The obtained limit of detection was 100 PFU/mL within the detection range of 102 – 5 × 104 PFU/mL for the H3N2 virus. The recovery yield was within the range of 97.6 to 98.1%.

Keywords: Sulfur-doped graphitic carbon nitride QDs, Silver disulfide nanocrystals, Influenza A virus, Fluoroimmunoassay, Virus immunoassay, localized surface plasmonic resonance, Nanosandwich complex.

Introduction

Influenza virus emerged as a major epidemic over a decade ago and has remained a growing challenge to public health that needs responsive and accurate diagnostic measures to prevent the spread of the virus and promote early treatment [1]. Therefore, the current gold-standard methods used for influenza virus immunoassays are enzyme-linked immunosorbent assay (ELISA), real-time reverse transcription-polymerase chain reaction (RT-qPCR), immunoblotting assays, and electrochemical sequence-specific genetic detection [2,3]. Although these methods offer specific advantages and are widely used, nevertheless, they suffer some drawbacks due to high operating costs and, in some cases, high interference by complex matrices. It is, therefore, still necessary to implement cost-effcient methods.

The exceptional optoelectrical properties of fluorescent graphic carbon nitride quantum dots (gCNQDs) have earned widespread interest for the design of promising fluorescent probes [4–6]. The synthesis of these carbon-based nanosized-particles encompasses the "top-down and "bottom-up" approaches. The latter approach, which is ubiquitously deployed, involves the advanced chemical treatments by condensation and/or controlled pyrolysis of small and organically rich molecules such as formamide, urea, diaminomaleonitrile, melamine, guanidine, dicyandiamide and organic amines [7–13]. Doping and/or hetero-atom functionalization of carbon-based graphitic QDs has helped to improve their optical and electronic properties for various applications. For

instance, sulfur-doped graphitic carbon nitride (gC_3N_4) nanosheets were prepared by the ball-milling of melamine and sulfur powder for 48 h and subsequently treated under hydrothermal condition. The obtained nanosheets were deployed for enhanced electrocatalytic activity in fuel cells [14]. Phenyl-modified gC_3N_4, which showed a stoke shift of ~185 nm and a high fluorescence (FL) intensity, was prepared and used as a probe for thiram, a pesticide [15]. In another reported study, an electrochemical sensor for ascorbic acid (AA), dopamine and uric acid was fabricated based on gC_3N_4 modified with graphene oxide [16]. A complex hybrid involving Cu-Pd nanoparticles was deposited on gC_3N_4 hybrid nanosheets for the colorimetric detection of glucose, taking advantage of the peroxidase mimic activity of the graphitic nanostructured composites [17]. In our previous studies, the facile one-step preparation of gCNQDs functionalized with thymine (T-gCNQDs) and tannic acid (TA-gCNQDs), respectively, were reported [9, 10]. The strongly fluorescent gCNQDs derivatives were deployed as highly competitive probes for Hg^{2+} and AA. However, innovative materials are still increasingly needed for the production of sensors/biosensors with real-time and realistic diagnostic applications. This ambition motivates the interest in the adoption of simple one-step *in situ* approaches for novel hybrid heteroatom-doped materials preparation.

In this work, the analytical application of novel S-gCNQDs was examined by the fluoroimmunoassay of the influenza A virus as a test analyte. A fluoroimmunosensing method was developed by utilizing the metal-induced

fluorescence enhancement of S-gCNQDs in the presence of Ag_2S nanocrystals (NCs). To develop the practical biosensor for influenza virus, novel S-gCNQDs and Ag_2S NCs, as innovative materials, were covalently conjugated to specific anti-human influenza A monoclonal antibodies for the capture of the target influenza A virus. An immuno-reaction ensued between the antibody-labeled S-gCNQDs/Ag_2S NCs in the presence of the influenza A virus. As a result, an immunocomplex structure was formed, followed by an enhancement of the fluorescence of the S-gCNQDs influenced by the proximity of Ag_2S NCs. The developed immunoassay is rapid and achieved a sensitive femtogram limit of detection (LOD) of 5.5 fg/mL for influenza A virus (H1N1). Also, clinically isolated influenza A virus (H3N2) was quantified down to 100 PFU/mL and shows that the developed system is highly sensitive compared to some commercially available rapid diagnostic test kits (with LODs of ~5000 PFU/mL). This system can be adapted for the versatile detection of other viral antigens by labeling the S-gCNQDs and Ag_2S NCs with suitable capture antibodies, which can induce the needed immunoreactions.

Experimental

Chemicals and biological reagents/materials

Silver nitrate ($AgNO_3$), 3-Mercaptopropionic acid (MPA, 99 %), dimethyl formamide (DMF), bovine serum albumin (BSA), Rhodamine 6G, N-

hydroxysuccinimide (NHS), and N-(3-dimethylaminopropyl)-N'-ethylcarbodiimide hydrochloride (EDC) were purchased from Sigma-Aldrich (St Louis, USA, https://www.sigmaaldrich.com/). 4-Amino-3-hydrazino-5-mercapto-1, 2, 4 triazole, Bovine serum albumin (BSA), 4-mercaptobenzoic acid (4-MBA) and NaOH were supplied by FUJIFILM Wako Pure Chemical Corporation (Osaka, Japan, http://ffwk.fujifilm.co.jp/en/index.html). Diethylene glycol (DEG) was purchased from Tokyo Chemical Industry (TCI) (Tokyo, Japan, https://www.tcichemicals.com/en/jp/).

Anti-human influenza A (H1N1) monoclonal antibody (clone C179), anti-human influenza A (H3N2) monoclonal antibody (Clone F49) and anti-human influenza A (H1, H2, H3) monoclonal antibody (Clone C111) which is positive for both influenza viruses H1N1 and H3N2 were purchased from Takara Bio. Inc (Kusatsu, Shiga, Japan, https://www.takara-bio.com/). Influenza virus A/New Caledonia (20/99/IVR/116) (H1N1) was purchased from ProSpec-Tany TechnoGene Ltd. (Rehovot, Israel, https://www.prospecbio.com/). Human Serum from human male AB plasma, USA origin, sterile-filtered was obtained from Sigma-Aldrich (St Louis, USA, https://www.sigmaaldrich.com/), Dengue virus DNA was supplied by Integrated DNA Technologies (Iowa, USA) (www.idtdna.com). Clinically isolated influenza virus A/Yokohama/110/2009 (H3N2) was kindly provided by Dr. C. Kawakami of Yokohama City Institute of Health, Japan. Goat anti-rabbit IgG-HRP were purchased from Santa Cruz Biotechnology (Dallas, Texas, USA, https://www.scbt.com/home). Commercial RIDT kit - *QuikNavi Flu 2* was

purchased from Denka -Seiken Co. Ltd. (Tokyo, Japan, http://denka-seiken.jp/jp/). For selectivity studies, Prof. K. Morita of Institute of Tropical Medicine, Nagasaki University, kindly provided the zika virus used in this study. Noro virus-like particles (NoV-LPs) were prepared in our lab, according to the previously reported protocol [18]. Hepatitis E virus-like particles (HEV-LPs) were prepared according to the previous report [19]. All experiments were carried out using high purity deionized (DI) water (>18 MΩ·cm). All detection/sampling protocol was carried out according to the standard protocol for influenza virus immunoassays [20].

Instrumentation

Ground state electronic absorption (UV/vis), fluorescence excitation and emission spectra were recorded on a filter-based multimode microplate reader (Infinite F200 M; TECAN, Ltd, Männedorf, Switzerland, https://www.tecan.com/). Images of the transmission electron microscope (TEM) were acquired using JEM-2100F operating at 100 kV (JEOL, Ltd., Tokyo, Japan, https://www.jeol.co.jp/en/products/detail/JEM-2100.html). Powder X-ray diffraction (PXRD) analysis was carried out using a RINT ULTIMA XRD (Rigaku Co., Tokyo, Japan, https://www1.rigaku.com/ja) with αNi filter and a Cu-Kα source. Data were collected over $2\theta = 15 - 60°$ at a scan rate of 0.01°/step and 10 s/point. Dynamic light scattering (DLS) analysis was done on a Malvern Zetasizer

nanoseries, Nano-ZS90 (Malvern Inst. Ltd., Malvern, UK, https://www.malvernpanalytical.com/). Fourier transform infrared spectroscopy was performed using FT/IR-6300 with ATR PRO610P-S (JASCO, Tokyo, Japan, https://www.jasco.co.jp/). Raman spectroscopic measurements and surface-enhanced Raman scattering (SERS) experiment of 4-MBA (Raman reporter) and the virus-immunocomplex using Ag_2S NCs as the SERS substrate were carried out using NRS-7100 Raman Spectrometer with f500 spectrograph (**JASCO, Tokyo, Japan)**. The measurements were done using a 20× objective lens at 1 % laser power and 2 s integration time. Fluorescence lifetime imaging microscopy (FLIM) experiment for lifetime determination was done using a Nikon Eclipse Ti-U microscope with a Nikon CFI S Plan Fluor ELWD 40x (NA=0.60) and Hamamatsu C8898 (Wavelength: 374 nm, Pulse width: 74 ps, peak power: 47mW) as the laser source (Hamamatsu, Japan). The FLIM camera used was a Lab-made camera with a custom CMOS image sensor. The images were acquired by the FLIM CMOS camera via the Framelink PCIe card (VCE-CLEX02). The FLIM CMOS camera has a pixel array of 128 x 128 pixels; each has a four-tap pixel with a pitch of 22.4 μm x 22.4 μm. The sensor response time is 170ps, measured with a 472 nm laser diode. Details of the Phasor plots generation are given in Electronic Supporting Information (ESM).Conjugation of the antibody to the individual nanoparticles was confirmed by enzyme-linked immunosorbent assay (ELISA) using a microplate (Model 680; Bio-Rad, Hercules, USA, https://www.bio-rad.com/en-us/).

Synthesis of S-gCNQDs

Sulfur-doped graphitic carbon nitride QDs (S-gCNQDs) were prepared by the solvothermal treatment of a novel precursor i.e., mercapto-based triazole compound (**Scheme 1**). Briefly, 4-Amino-3-hydrazino-5-mercapto-1, 2, 4 triazole (50 mg), and citric acid (5 mg) were dissolved in 10 mL of DMF, and the mixture was sonicated for 20 min to obtain a suspension. The resulting mixture was transferred and sealed in a 50 mL Teflon-lined stainless steel autoclave and heated at 200 °C for 8 h. The autoclave was allowed to cool naturally, and the obtained product was filtered through a 0.22 μm microporous filter membrane and then dialyzed for 2 d using a dialysis tubing membrane - MWCO 2.0 kDa to obtain pure S-gCNQDs solution. The solution was further freeze-dried to get a solid product.

Ag_2S NCs were synthesized according to procedures reported previously with some modification [21]. Detailed synthesis procedures are presented in Electronic Supporting Information (ESM).

Antibody conjugation process and virus detection

Firstly, anti-human influenza virus A (H1N1) (Clone C179) or (H1, H2, H3) (Clone C111) monoclonal antibody was conjugated onto the surface of S-gCNQDs or Ag_2S NCs via EDC/NHS chemistry. To achieve this, 100 μL of 0.1 M EDC was added to 2 mL (0.1 mg/mL) of S-gCNQDs to activate the carboxylic groups on their surface,

and the solution was stirred for 1 h, following by the addition of 100 μL of 0.1 M NHS to the mixture and the stirring continued for another 1 h. Then 5.1 μg/mL of the antibody (prepared in PBS 7.6) was added to the activated S-gCNQDs, and the resulting mixture was stirred for 8 h at 7 °C. Anti-human influenza virus A (H3N2) monoclonal antibody (Clone F49) was also conjugated to S-gCNQDs for the detection of the clinically isolated influenza virus A/Yokohama/110/2009 (H3N2). Similar procedures were followed for the antibody conjugation of the Ag_2S NCs, but using anti-human influenza virus A (H1, H2, H3) (Clone C111) monoclonal antibody instead of anti-human influenza virus A (H1N1) (Clone C179). The obtained antibody-conjugated S-gCNQDs or Ag_2S NCs were purified by centrifugation (3000 × g, 5 min) to remove unbound antibodies followed by incubation with 5 % BSA (for blocking) to ensure non-specific binding interactions. Excess BSA was further removed by centrifugation, and the conjugates redissolved in ultra-pure DI water for further use.

Following the antibody conjugation, the virus assay was carried out using different concentrations of influenza A virus (H1N1) within the range from 1.0 fg/mL to 10 ng/mL. Typically, in a 96-well plate, 100 μL of the antibody-conjugated S-gCNQDs (2.0 mg/mL in PBS, pH 7.6) was incubated with 100 μL of each concentration (1, 10, 10^2, 10^3, 10^4, 10^5, 10^6 fg/mL) of the influenza A/New Caledonia virus (H1N1) for 2 min. Then 50 μL of the antibody-conjugated-Ag_2S (1 mg/mL in PBS, pH 7.6) was added to the mixture and shaken for 5 min to induce the virus-mediated nanosandwich complex formation. Then the FL intensity

214 change of the S-gCNQDs in the hybrid sandwich nanostructure was measured at
215 400 nm excitation wavelength, with maximum emission intensity at 512 nm to
216 construct a calibration curve.

217 The analysis of clinically isolated influenza A/Yokohama (H3N2) was assayed
218 using similar procedures upon mixing with human serum. 100 µL of the antibody-
219 conjugated S-gCNQDs (2.0 mg/mL in PBS, pH 7.6) was mixed with 50 µL of the
220 clinical samples dissolved in PBS (pH 7.6) in 40 % diluted human serum and
221 incubated for 2 min. This solution was followed by the addition of 50 µL of the
222 antibody-conjugated-Ag_2S NCs (1 mg/mL in PBS, pH 7.6) and then thoroughly
223 shaken for 5 min and allowed for about further 10 min before the FL signals were
224 collected at 512 nm emission wavelength upon excitation at 400 nm. The
225 detected range was within 20 – 50,000 PFU/mL of the clinical samples. All
226 detection experiments were done in triplicate under a similar procedure and at
227 optimized conditions (See ESM for details).

228

229 ## Results and discussion

230 ### Choice of materials

231 The surface functionalization and/or doping of carbon-based QDs with
232 heteroatoms (S, N, and B) are known to result in substantial improvements in
233 their optical properties and performance [22–24]. This is because their optical
234 properties are altered by the introduction of "emissive trap sites" and/or "surface

defects," which influence the radiative recombination of their excitons [25, 26]. This work presents an exceptionally rich novel source precursor for the preparation of gCNQDs with heteroatoms (S and N) functionality using 4-Amino-3-hydrazino-5-mercapto-1, 2, 4 triazole. This compound contains a high percentage of the amino group (NH_2) (essential for covalent attachments) and N-atoms linked in a triazole ring with extended C-N and C=S linkages (**Scheme 1**). The S, N-derived gCNQDs herein has a significant advantage which is the connective affinity to interact with Au or Ag-based nanoparticles to form functional hybrids. In addition to the presence of a planar graphitic structure for non-covalent π stacking interactions, S-gCNQDs prepared using this precursor possesses more than one point of attachment for simple surface modifications and hybrid nano-structuring choices.

On the other hand, plasmonic semiconductor nanostructures can act as nanoantennas when close to fluorophores resulting in changes in their optical properties. This mostly leads to a favorable effect known as metal-enhanced fluorescence (MEF) [27–29]. This type of influence has been used in detection systems where metallic nanostructures regulate the emissions of colloidal quantum dots [28]. Semiconductor nanocrystals such as Ag_2S NCs used in this work, are known to exhibit tunable plasmonic properties in the near-infrared (NIR) region and are excellent nanostructures for various optical-based signal enhancement processes such as MEF, SERS, and photocatalysis [28–32]. It is in this light that we deployed Ag_2S NCs in this work to push the fluorescence detection sensitivity of S-

gCNQDs for the detection of influenza virus via metal-based enhancement of their fluorescence by controlling the local environment surrounding the S-gCNQDs via immunoreactions with influenza virus, as a test analyte.

Synthesis and characterization of novel S-gCNQDs and Ag_2S nanocrystals

The precursor for the S-doped gCNQDs was 4-amino-3-hydrazino-5-mercapto-1, 2, 4 triazole. This precursor was inspired by its high nitrogen/sulfur content and relatively low cost. Hence, the solvothermal treatment and condensation of the heterocyclic triazole ring of the precursor to achieving novel S-gCNQDs follows a similar formation mechanism as outlined in literature for the synthesis of gCNQDs using other triazole compounds [7, 8, 12, 13].

To characterize the prepared S-gCNQDs, TEM was employed, and the image acquired shows a quasi-spherical morphology of the S-gCNQDs. They appear to be monodispersed with sizes typically estimated within the range of 3–5 nm (**Fig. 1A**). To supplement the information on the size determination from the TEM micrograph, the DLS experiment revealed that the average size distribution of the gCNQDs was ~5.5 nm (**Fig. 1B**). This result is in close agreement with the size distribution obtained using TEM images, and further indicates sizes typical of carbon-based QDs [7, 9, 10]. XRD pattern obtained for the S-gCNQDs displayed a broad diffraction peak at $2\theta = 27^{0}$, which is indexed as (002) lattice typical of graphitic carbon nitrides (g-C_3N_4) (**Fig. 2A**) [7, 12, 13]. This diffraction peak

corresponds well in intensity and position with the known d-spacing and disordered nanostructure of g-C_3N_4, thus indicating their formation. Fourier transform infrared (FTIR) spectroscopy further revealed the base structure of the S-doped gCNQDs derivative. As shown in **Fig. 2B**, the observed vibration at 662 cm^{-1} is assigned to the formed heptazine units of the S-gCNQDs. Characteristic absorption bands of C=N/C-C and C-N stretching modes of the graphitic structure were observed at 1493, 1387, and 1097 cm^{-1}, respectively. At 1628 cm^{-1}, asymmetric vibrations referring to the carboxylic groups introduced by citric acid as co-precursor is conspicuously observed. Intense broad peak typical of the –N-H (resulting from the 2^0 or 3^0 amine moieties) and/or hydroxyl (OH) of the carboxylic group vibrations have been observed around 3715-2985 cm^{-1} as well as characteristic $-CH_2$ peaks of the triazine rings at 2930 and 2897 cm^{-1}. The presence of the S-atom was confirmed by the appearance of a strong C=S absorption at 1248 cm^{-1}, with an accompanying weak vibration of the C-S bond at 859 cm^{-1} (**Fig. 2B**). The Raman spectra (**Fig. 2C**) of the solvothermally prepared S-gCNQDs displayed the characteristic bands indexed at ~1345 (D band) and ~1586 cm^{-1} (G band) due to the disordered sp^2 as a result of the C-N linkage and graphitic sp^2 layer nanostructures, respectively [7–10, 12, 13]. These results confidently show that S-gCNQDs were successfully prepared using the novel precursor.

The ground-state absorption recorded for the prepared S-gCNQDs is reminiscent of the electronic transition (π - π*) of the s-triazine units of the carbon nitride family [33–35]. An intense absorption occurred in the region <500 nm.

Therefore, the S-gCNQDs were subjected to different excitation wavelengths (350 to 500 nm) to determine the optimum emission intensity and wavelength. At an excitation wavelength of 400 nm, the emission intensity was maximum and occurred at ~512 nm. Next, the evaluation of the relative fluorescence quantum yield (Φ_F) of the material was calculated to be ~33 % using Rhodamine 6G as the reference standard (see Electronic Supporting Information for details). The value of Φ_F for the prepared S-gCNQDs (using 4-amino-3-hydrazino-5-mercapto-1, 2, 4 triazole as the source of S and N) is higher than that reported using other source precursors such as urea (17.9 %), melamine (5.5 %) or formamide (29 %) [7, 36, 37]. It is demonstrated in this work that the use of 4-amino-3-hydrazino-5-mercapto-1, 2, 4 triazole results in a graphitic QDs with FL emission extending into the green region of the visible spectrum which are desired for various applications.

Further, fluorescence lifetime imaging microscopy (FLIM) experiments were conducted to determine the lifetime of the prepared S-gCNQDs. This measurement was carried out using the frequency-domain FL lifetime determination known as the Phasor approach [38, 39]. This approach, which differs from time-correlated single-photon counting method, is accomplished by analyzing the FLIM data in Phasor space by observing the clustering of pixel values (from images) in some areas of the generated Phasor plots rather than by fitting the fluorescence decay using exponentials. As is shown in **Fig. 3A**, the second (*), and third (#) peaks from the measured waveform are due to crosstalk between different taps in the pixel of the acquired images. This is then deconvoluted to

obtain the result, **Fig. 3B**. The average value of the two-component decay lifetime of S-gCNQDs was determined to be 3.19 ns. The FLIM measurement results of S-gCNQDs and their immunocomplexes in the presence of the target virus are shown in Fig. S3 in Electronic Supporting Information (ESM).

Detailed Ag_2S NCs characterization data, experimental results demonstrating their plasmonic/optical properties, and discussion are presented in Electronic Supporting Information (ESM).

Sensitive fluoroimmunoassay

Influenza A/New Caledonia virus (H1N1) was detected based on preliminary studies using Ab-conjugated S-gCNQDs in the presence of Ab-Ag_2S NCs to form a nanosandwich complex leading to signal-amplified fluorescence cycles which are dependent on the concentrations of the target influenza virus A(H1N1) (**Fig. 4A**). The Influenza A virus (H1N1) detection was initially carried out in DI water, and the recorded FL intensities are shown in **Fig. 4A**. Also, since the human serum is a mixture of complex biological compounds as matrices, the influenza A/New Caledonian (H1N1) virus was assayed in human serum (40 %) to simulate the conditions close to actual clinical samples. Hence, it was observed that the S-gCNQDs could respond to the presence of the influenza A virus (H1N1) within the linear concentration range of 10 fg/mL to 1 ng/mL (**Fig. 4B**). The detection

sensitivity of the probe towards the target virus (H1N1) was evaluated by the construction of a calibration plot using Eqn. 1 [40].

$$\frac{\Delta F}{F_0} = \mathbf{0.1} + \mathbf{K}[\mathbf{Virus}] \qquad (1)$$

where ΔF is the difference between FL intensity before (F_0) and after (F) addition of virus, K is the fluorescence enhancement factor. [Virus] is the concentration of the target virus. The expression $\Delta F/F_0 = (F_{\text{with virus}} - F_0)/F_0$ gives a ratio of the fluorescence enhancement to the fluorescence signal before virus addition (F_0) [41].

Overall, the increased concentrations of influenza A virus (H1N1) led to a proportional enhancement in the FL intensity of S-gCNQD measured in DI water and human serum, respectively. Interestingly, the sensitivity achieved in both media showed an only but slight difference, with similar linearity of their calibration plots (**Fig. 4B**). The analytical figures of merit of the assay were assessed by calculating the limits of detection (LODs) using the equation (LOD = 3δ/K) [42], where the standard deviation (δ) of 10 replicated measurements (n = 10) was taken. K is the value of the slopes of the linear calibration plots. The LOD was calculated to be 5.5 fg/ml in DI water and 8.5 fg/ml in human serum, respectively (**Table S1**).

Detailed results and discussion of optimization and control studies leading to the established detection of influenza virus in work are given in the Electronic Supporting Information (ESM).

Assay of clinically isolated influenza virus (H3N2)

To detect clinically isolated influenza A virus (H3N2), the S-gCNQDs modified with the H3N2 monoclonal antibody was employed (instead of H1N1 monoclonal antibody) in the presence of the Ab-Ag_2S NCs to form a sandwich nanocomplex. It was observed that the Ab (H3N2)-conjugated S-gCNQDs responded to the presence of the influenza A virus (H3N2) within the linear concentration range of 100–50000 PFU/mL (**Fig. 5A**). The detection sensitivity of the probe towards clinically isolated influenza A virus (H3N2) was evaluated by the construction of a calibration plot (**Fig. 5A inset**), using Eqn. (1) above. The calculated LOD was 100 PFU/mL. Also, human serum was spiked with a known concentration of the clinically isolated influenza A (H3N2). The assay was able to quantify ~98 % of the virus with good recoveries (**Table S2**). Therefore, the performance of the developed detection platform for the influenza virus was further evaluated against a commercial rapid influenza diagnostic kit (RIDT) – *QuikNavi-Flu* 2 (Denka Seiken Co. Ltd, Tokyo, Japan). The clinical samples assayed using the RIDT showed that influenza virus A/Yokohama/110/2009 (H3N2) samples with ≥1000 PFU/mL could only be detected. As shown in Fig. S4, influenza virus A/Yokohama/110/2009 (H3N2) is not detectable at <1000 PFU/mL by the RIDT kit). Meanwhile, our developed biosensor for the influenza virus is responsive to the H3N2 viral RNA down to 45 PFU/mL. This result indicates that our detection system can achieve an upwards of ~10 times more

sensitivity when used in place of the commercial RIDT. It should be pointed out, however, that both detection strategies are, in theory, very different, and the production of a fast diagnostic kit with our designed system will enhance the sensitive detection of the influenza virus considerably. Furthermore, clinical samples containing target influenza virus can be assayed rapidly in ~ 15 min, which is quite preferable to the clinical used RT-PCR or rapid molecular assays capable of producing results in approximately 15-30 min, and other molecular assays capable of detecting RNA or nucleic acid influenza in around 45–80 min [2, 3].

Selectivity

The selectivity of the developed assay was probed in the presence of NoV-LPs, Zika virus, HEV-LPs, and Dengue DNA to establish the extent of the selective nature of the test. Expectedly, no interferences and/or changes occurred in the fluorescence signal of S-gCNQDs even to 1 ng/mL of the tested virus and VLPs (**Fig 5B**). This observation can be attributed to the specific affinity of the influenza A virus to bind to the antibody functionalized nanoparticles (S-gCNQDs/Ag_2S NCs). This affinity is as a result of the induced changes in the FL intensity of the S-gCNQDs signals compared to when other non-specific viruses interact with S-gCNQDs. It is pertinent to state here that this system may present a versatile detection approach for desired viruses by choosing the appropriate antigen-

antibody pair for the sandwich immuno-reactions leading to the sensitive detection of the mediating virus.

However, the proposed assay herein has some limitations. The sensitivity of this assay is majorly limited by the interference of heavy metals such as Hg^{2+} and Cd^{2+} ions, which can quench the FL of the S-gCNQDs. Also, the sizes of the S-gCNQDs and Ag_2S NCs may need to be carefully controlled to achieve the sandwich formation in the presence of the target virus. Clinical samples matrix interference may impair the sensitivity of detection. To address this, a magnetic separation protocol/virus enrichment should be considered.

Detection mechanism

In view of the observed FL enhancement in S-gCNQDs when immunocomplex with influenza virus in the presence of Ag_2S NCs, it was speculated that aggregation-induced emission and/or metal-plasmonic enhancement effects might be responsible for the FL signal enhancement. However, results obtained from the TEM image of the immunocomplex (Fig. S5 in Electronic Supporting Information), showed no clear evidence of aggregation of nanoparticles of S-gCNQDs or Ag_2S NCs in the presence of the target virus. This outcome diverted our attention to the possibility of an optical-based enhancement mechanism since the plasmonic properties of Ag_2S NCs have been reported previously [43, 44]. Raman measurement and SERS analysis were carried out (detailed results and discussion

426 are presented in Electronic Supporting Information). To elucidate the detection
427 mechanism of the developed immunoassay by evaluating the plasmonic and/or
428 optoelectronic coupling effects of Ag_2S NCs, the SERS experiments were carried
429 out further complement the observed FL enhancement of S-gCNQDs (Fig. 6), the
430 detailed SERS results and discussion of 4-MBA are shown in Fig. S6 of Electronic
431 Supporting Information. The results plausibly demonstrated that the coupling
432 interactions between S-gCNQDs and Ag_2S NCs via plasmonic and/or chemical
433 interaction resulted in the observed SERS signal enhancement of S-gCNQDs,
434 similar to report for GQDs in the presence of plasmonic nanostructures [45].
435 Therefore, it is credible to state that the enhanced SERS signals from the S-
436 gCNQDs/Ag_2S NCs virus-mediated immunocomplex are due to the local optical
437 field created by electronic interaction between the S-gCNQDs and Ag_2S NCs. This
438 process might be responsible for the enhancement of the fluorescence signals of
439 the S-gCNQDs resulting from their proximity to Ag_2S NCs in a sandwiched
440 network triggered by the target virus (**Scheme 2**). Overall, these findings and the
441 control experiments lead us to conclude that Ag_2S NCs influenced the
442 enhancement of the fluorescence of S-gCNQDs regulated by the target influenza
443 virus, which resulted in the sensitive detection of the virus.

444 ## Conclusion

445 In this work, a functional and innovative combination of S-doped graphitic QDs
446 and Ag_2S nanocrystals are deployed for the fluoroimmunoassay of influenza A
447 virus. The S-doped graphitic QDs, which were prepared using a novel precursor

via a rapid one-step solvothermal route, displayed excellent optical properties. Their functionalization with specific antibodies positive for the target virus, initiated a virus-regulated interaction between the S-doped graphitic QDs and Ag_2S nanocrystals . This resulted in the fluorescence enhancement of S-gCNQDs upon forming an immunocomplex with the influenza virus in the presence of Ag_2S nanocrystals. The fluorescence of S-gCNQDs increased consistently as the concentration of the virus increased, thus leading to the rapid detection of the target influenza virus in a highly sensitive and selective manner. The materials herein present an opportunity to fabricate a novel biosensing platform required for practical detection of the influenza virus and for testing other potentially harmful infectious diseases. This assay is rapid, convenient, and versatile as specific proteins and virus-like particles of clinical interests can conceivably be expanded when the materials are functionalized with capture antibody of interest.

Acknowledgment/Funding

The authors sincerely thank Professor K. Morita of the Institute of Tropical Medicine, Nagasaki University, for providing the Zika virus. Dr. C. Kawakami of Yokohama City Institute of Health, Japan, is gratefully acknowledged for providing the clinically isolated influenza virus A/Yokohama/110/2009 (H3N2). We also wish to thank Dr. T.C. Li of the National Institute for Infectious Disease of Japan for providing HEV-LPs. O.J.A and S. K. gratefully acknowledge the Japan Society for the Promotion of Science (JSPS) for a Postdoctoral Fellowship for

Research in Japan (Standard) (Grant No. 19F19348) and the Grant-in-Aid for Scientific Research (S) (Grant No. 18H05240), respectively.

Competing interests

None declared.

Ethical approval

This study was approved and carried out according to the guidelines provided by the Ethics Committee of the Environment and Hygiene Institute in Shizuoka Prefecture (September 14, 2016).

References

1. Gatherer G (2009) The 2009 H1N1 influenza outbreak in its historical context. J. Clin. Virol. 45:174-178

2. Dziąbowska K, Czaczyk E, Nidzworski, D (2018) Detection Methods of Human and Animal Influenza Virus-Current Trends. Biosensors, 8:94. https://doi.org/10.3390/bios8040094

3. Choi YJ, Kim HJ, Park JS, Oh MH, Nam HS, Kim YB (2010) Evaluation of new rapid antigen test for detection of pandemic influenza A/H1N1 2009 virus. J. Clin. Microbiol. 48:2260–2262. https://doi.org/10.1128/JCM.02392-09

4. Dong Y, Wang Q, Wu H, Chen Y, Lu CH, Chi Y, Yang HH (2016) Graphitic carbon nitride materials: sensing, imaging and therapy. Small 12:5376–5393

5. Ahmad R, Tripathy N, Khosla A, Khan M, Mishra P, Ansari WA, Syed MA, Hahn YB (2020) Recent Advances in Nanostructured Graphitic Carbon Nitride as a Sensing Material for Heavy Metal Ions. *J. Electrochem. Soc.* **167**:037519

6. Cheng Q, He Y, Ge Y, Zhou J, Song G (2018) Ultrasensitive detection of heparin by exploiting the silver nanoparticle-enhanced fluorescence of graphitic carbon nitride (g-C_3N_4) quantum dots. Microchim Acta 185:332–340

7. Barman S, Sadhukhan M (2012) Facile bulk production of highly blue fluorescent graphitic carbon nitride quantum dots and their application as

highly selective and sensitive sensors for the detection of mercuric and iodide ions in aqueous media. J Mater Chem 22:21832–21837

8. Tang Y, Su Y, Yang N, Zhang L, Lv Y (2014) Carbon nitride quantum dots: a novel chemiluminescence system for selective detection of free chlorine in water, Anal Chem 86:4528-4535

9. Achadu OJ, Revaprasadu N (2019) Tannic acid-derivatized graphitic carbon nitride quantum dots as an "on-off-on" fluorescent nanoprobe for ascorbic acid via copper(II) mediation. Microchim Acta 186:87-97. https://doi.org/10.1007/s00604-018-3203-x

10. Achadu OJ, Revaprasadu N (2018) Microwave-assisted synthesis of thymine-functionalized graphitic carbon nitride quantum dots as fluorescent nanoprobe for mercury(II). Microchim Acta 185:461–469

11. Xu J, Chen Y, Ma D, Shang JK, Li YX (2017) Simple preparation of MgO/g-C_3N_4 catalyst and its application for catalytic synthesis of dimethyl carbonate via trans-esterification. Catal Commun 95:72-76

12. Li Y, Cai J, Liu F, Yu H, Lin F, Yang H, Lin Y, Li S (2018) Highly crystalline graphitic carbon nitride quantum dots as a fluorescent nanosensor for detection of Fe(III) via an inner filter effect. Microchim Acta 185:134-140

13. Liu S, Tian J, Wang L, Luo Y, Sun X (2012) A general strategy for the production of photoluminescent carbon nitride dots from organic amines

and their application as novel peroxidase-like catalysts for colorimetric detection of H_2O_2 and glucose. RSC Adv 2:411-413

14. Xu C, Han Q, Zhao Y, Wang L, Li· Y, Qu L (2015) Sulfur-doped graphitic carbon nitride decorated with graphene quantum dots for an efficient metal-free electrocatalyst. J Mater Chem A 3:1841-1846

15. Mei H, Shu H, Lv H, Liu MW, Wang X (2020) Fluorescent assay based on phenyl-modified *g*-C_3N_4 nanosheets for determination of thiram. Microchim Acta 187:159-167

16. Zhang L, Liu C, Wang Q, Wang X, Wang, S (2020) Electrochemical sensor based on an electrode modified with porous graphitic carbon nitride nanosheets (C_3N_4) embedded in graphene oxide for simultaneous determination of ascorbic acid, dopamine and uric acid. Microchim Acta 187: 149-159. https://doi.org/10.1007/s00604-019-4081-6

17. Darabdhara, G, Boruah PK, Das MR (2019) Colorimetric determination of glucose in solution and via the use of a paper strip by exploiting the peroxidase and oxidase mimicking activity of bimetallic Cu-Pd nanoparticles deposited on reduced graphene oxide, graphitic carbon nitride, or MoS_2 nanosheets. Microchim Acta 186:13-23. https://doi.org/10.1007/s00604-018-3112-z

18. Ahmed SR, Takemura K, Li TC, Kitamoto N, Tanaka T, Suzuki T, Park EY (2017) Size-controlled preparation of peroxidase-like graphene-gold nanoparticle hybrids for the visible detection of norovirus-like particles. Biosens. Bioelectron. 87:558-565

551 **19.** Li TC, Yamakawa Y, Suzuki K, Tatsumi M, Razak M, Uchida T, Takeda N,
552 Miyamura T (1997) Expression and self-assembly of empty virus-like
553 particles of hepatitis E virus. J Virol 71:7207-7213.
554 **20.** World Health Organization (2017) **WHO information for the molecular**
555 **detection of influenza viruses** July [accessed 5 June 2020]
556 http://www.who.int/influenza/gisrs_laboratory/WHO_information_for_the
557 _molecular_detection_of_influenza_viruses_20171023_Final.pdf
558 **21.** Jiang P, Zhu CN, Zhang ZL, Tian ZQ, Pang DW (2012) Water-soluble Ag_2S
559 quantum dots for near-infrared fluorescence imaging in vivo. Biomaterials
560 33:5130-5135
561 **22.** Bankole OM, Achadu OJ, Nyokong T (2017) Nonlinear Interactions of
562 Zinc Phthalocyanine-Graphene Quantum Dots Nanocomposites:
563 Investigation of Effects of Surface Functionalization with Heteroatoms. J
564 Fluoresc 27:755–766
565 **23.** Qu D, Zheng M, Du P, Zhou Y, Zhang L, Li D, Tan H, Zhao Z, Xied Z, Sun
566 Z (2013) Highly luminescent S, N co-doped graphene quantum dots with
567 broad visible absorption bands for visible light photocatalysts. Nanoscale
568 5:12272–12277.
569
570 **24.** Holá K, Sudolská M, Kalytchuk S, Nachtigallová D, Rogach AL, Otyepka M,
571 Zbořil R (2017) Graphitic Nitrogen Triggers Red Fluorescence in Carbon
572 Dots. ACS Nano. 12:12402-12410

573 **25.** Gu SY, Hsieh CT, Gandomi YA, Chang JK, Li, J, Li JL, Zhang HA, Guo Q,
574 Lau KC, Pandey R (2019) Microwave Growth and Tunable
575 Photoluminescence of Nitrogen-doped Graphene and Carbon Nitride
576 Quantum Dot. J Mater Chem C 7:5468-5476
577 **26.** Wang J, Cao S, Ding Y, Ma F, Lu W, Sun M (2016) Theoretical
578 Investigations of Optical Origins of Fluorescent Graphene Quantum Dots.
579 Sci Rep 6:24850-24855
580 **27.** Lakowicz JR, Ray K, Chowdhury M, Szmacinski H, Fu Y, Zhang J,
581 Nowaczyk K (2008) Plasmon-controlled fluorescence: a new paradigm in
582 fluorescence spectroscopy Analyst, 133: 1308-1346
583 **28.** Deng W, Xie F, Baltar HTMCM, Goldys EM (2013) Metal-enhanced
584 fluorescence in the life sciences: here, now and beyond. Phys. Chem. Chem.
585 Phys., 15:15695-15708
586 **29.** Faucheaux JA, Stanton ALD, Jain PK (2014) Plasmon Resonances of
587 Semiconductor Nanocrystals: Physical Principles and New Opportunities. J.
588 Phys. Chem. Lett. 5:976-985. https://doi.org/10.1021/jz500037k
589 **30.** Lee SH, Nishi H, Tatsuma T (2017) Tunable plasmon resonance of
590 molybdenum oxide nanoparticles synthesized in non-aqueous media, Chem.
591 Commun. **53**:12680-12683

592 **31.** Zhang J, Pan Y, Chen Y, Lu H (2018) Plasmonic molybdenum trioxide
593 quantum dots with noble metal-comparable surface enhanced Raman
594 scattering, J. Mater. Chem. C. 6:2216-2220

595 **32.** Zhou Y, Li W, Zhang Q, Yan S, Cao Y, Dong F, Wang F (2017) Non-noble
596 metal plasmonic photocatalysis in semimetal bismuth films for
597 photocatalytic NO oxidation. Phys. Chem. Chem. Phys. 19:25610-
598 25616. https://doi.org/10.1039/C7CP04359G

599 **33.** Achadu OJ, Nyokong T (2017) *In situ* one-pot synthesis of graphitic
600 carbon nitride quantum dots and its 2, 2, 6, 6-tetramethyl (piperidin-1-yl)
601 oxyl derivatives as fluorescent nanoprobes for ascorbic acid. Anal Chim
602 Acta 991:113–126

603 **34.** Zhou J, Yang Y, Zhang CY (2013) A low-temperature solid-phase method
604 to synthesize highly fluorescent carbon nitride dots with tunable emission.
605 Chem Commun 49:8605-8607

606 **35.** Liu S, Wang L, Tian J, Zhai J, Luo Y, Lu W, Sun X (2011) Acid-driven
607 microwave-assisted production of photoluminescent carbon nitride from
608 N,N-dimethylformamide. RSC Adv 1:951-953

609 **36.** Guo J, Lin Y, Huang H, Zhang S, Huang T, Weng W (2017) One-pot
610 fabrication of fluorescent carbon nitride nanoparticles with high crystallinity
611 as a highly selective and sensitive sensor for free chlorine. Sensors and
612 actuators B: chemical 244:965–971

613 **37.** Rong M, Lin L, Song X, Wang Y, Zhong Y, Yan J, Feng Y, Zeng X, Chen X
614 (2015) Fluorescence sensing of chromium (VI) and ascorbic acid using
615 graphitic carbon nitride nanosheets as a fluorescent switch. Biosens.
616 Bioelectron 68:210–217
617 **38.** Digman MA, Caiolfa VR, Zamai M, Gratton E (2008) The phasor
618 approach to fluorescence lifetime imaging analysis. Biophys J 94:14–16
619 **39.** Chen H, Ma N, Kagawa K, Kawahito S, Digman M, Gratton E (2018)
620 Wide-field multi-frequency fluorescence lifetime imaging using a two-tap
621 complementary metal-oxide semiconductor camera with lateral electric
622 field charge modulators. J Biophotonics 12:1–9
623 **40.** Lakowicz JR (2009) Principles of fluorescence spectroscopy, Third edn.
624 Springer, New York, p 243
625 **41.** Lee J, Ahmed SR, Oh S, Kim J, Suzuki T, Parmar K, Park S, Lee J, Park EY
626 (2015) A plasmon-assisted fluoro-immunoassay using gold nanoparticle-
627 decorated carbon nanotubes for monitoring the influenza virus, Biosens.
628 Bioelectron. 64:311-317
629 **42.** Lima KMG, Raimundo Jr IM, Pimentel MF (2007) Improving the detection
630 limits of near infrared spectroscopy in the determination of aromatic
631 hydrocarbons in water employing a silicone sensing phase, Sens. Actuators
632 B Chem 125:229-233

633 **43.** Hou X, Zhang X, Yang W, Liu Y, Zhai X (2012) Synthesis of SERS active
634 Ag_2S nanocrystals using oleylamine as solvent, reducing agent and stabilizer.
635 Mater Res Bull 47:2579–2583

636 **44.** Fang C, Lee YH, Shao L, Jiang R, Wang J, Xu QH (2013) Correlating the
637 Plasmonic and Structural Evolutions during the Sulfidation of Silver
638 Nanocubes. ACS Nano, 7:9354–9365. doi:10.1021/nn404042p

639 **45.** Zou F, Zhou H, Van Tan T; Kim J, Koh K, Lee J (2015) Dual-Mode SERS-
640 Fluorescence Immunoassay Using Graphene Quantum Dot Labeling on
641 One-Dimensional Aligned Magnetoplasmonic Nanoparticles. *ACS Appl.*
642 *Mater. Interfaces* 7:12168–12175. https://doi.org/10.1021/acsami.5b02523

643

644

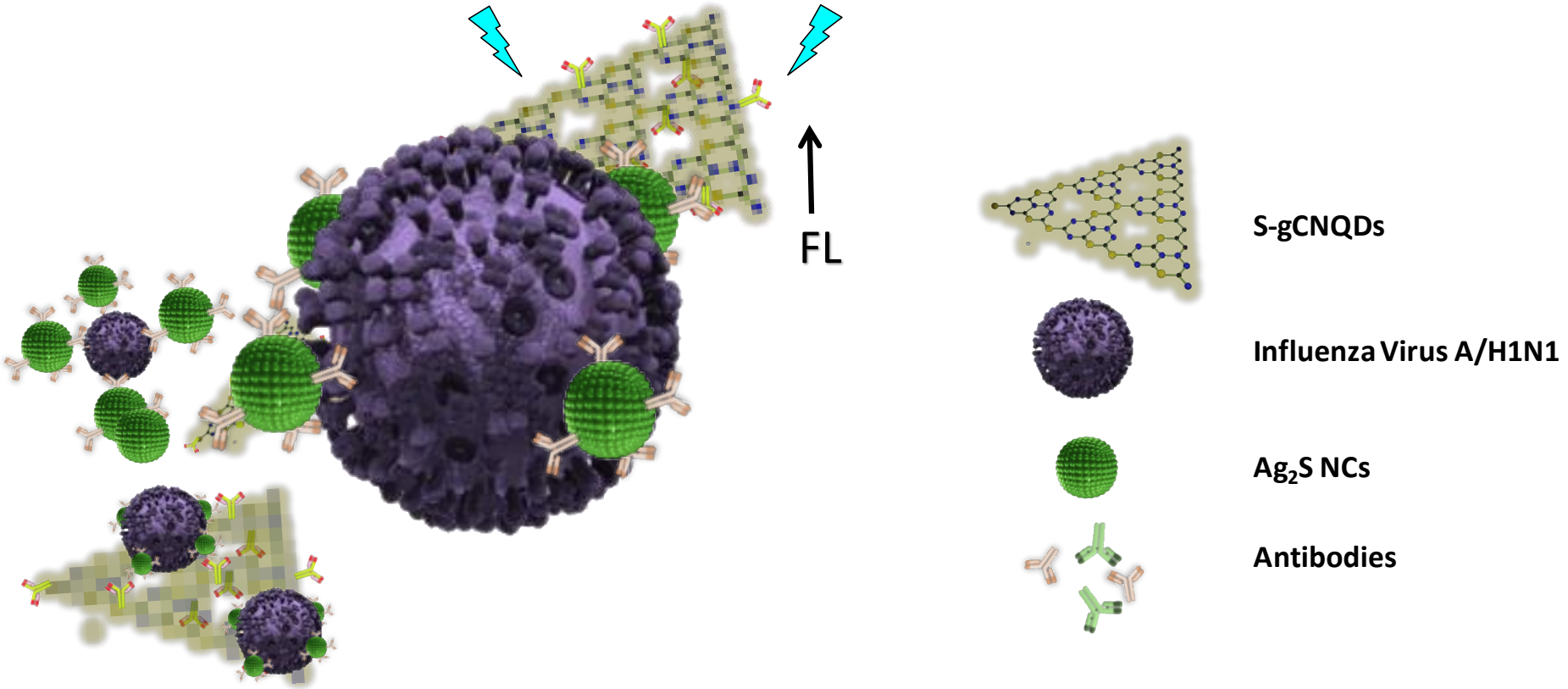
FL
S-gCNQDs
Influenza Virus A/H1N1
Ag_2S NCs
Antibodies

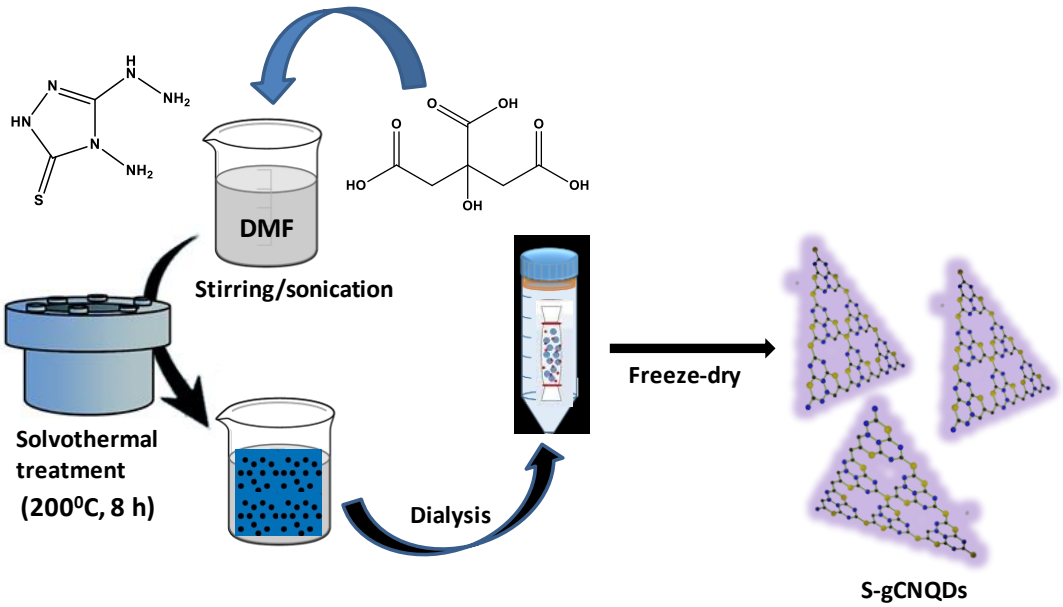

Scheme 1. Synthesis pathway of S-gCNQDs.

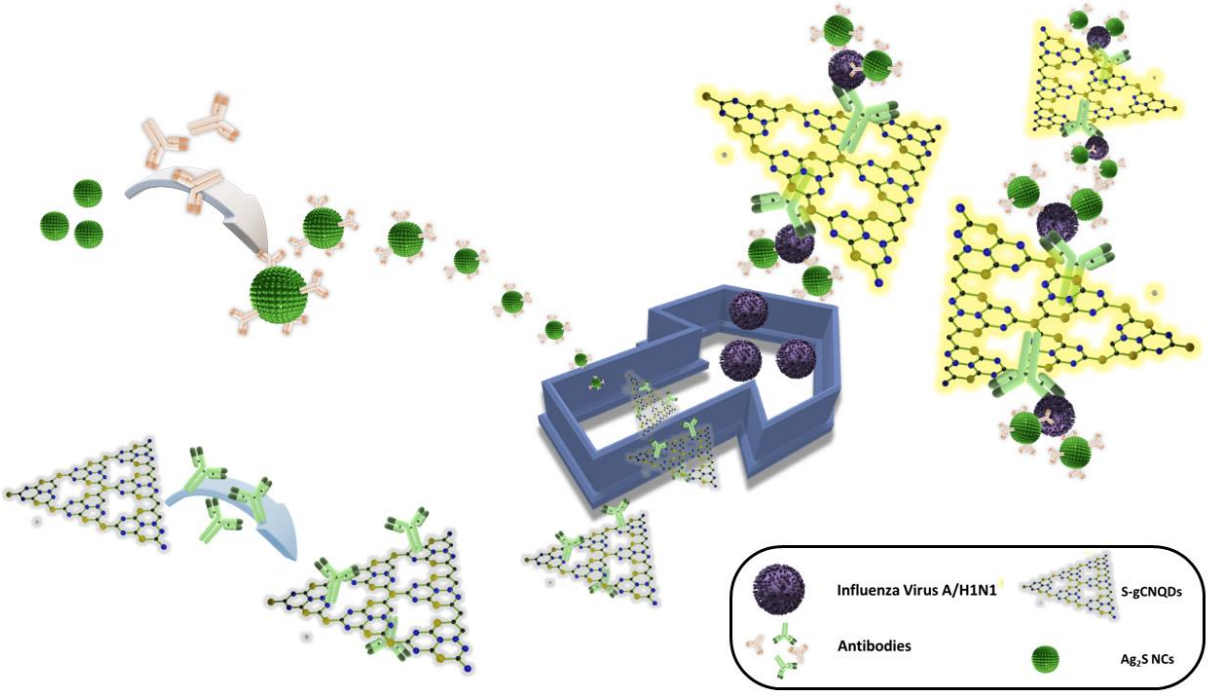

Scheme 2. Schematic representation of the S-gCNQDs and Ag_2S modification with antibody and the detection protocol by sandwich nanostructure formation in the presence of target influenza A virus.

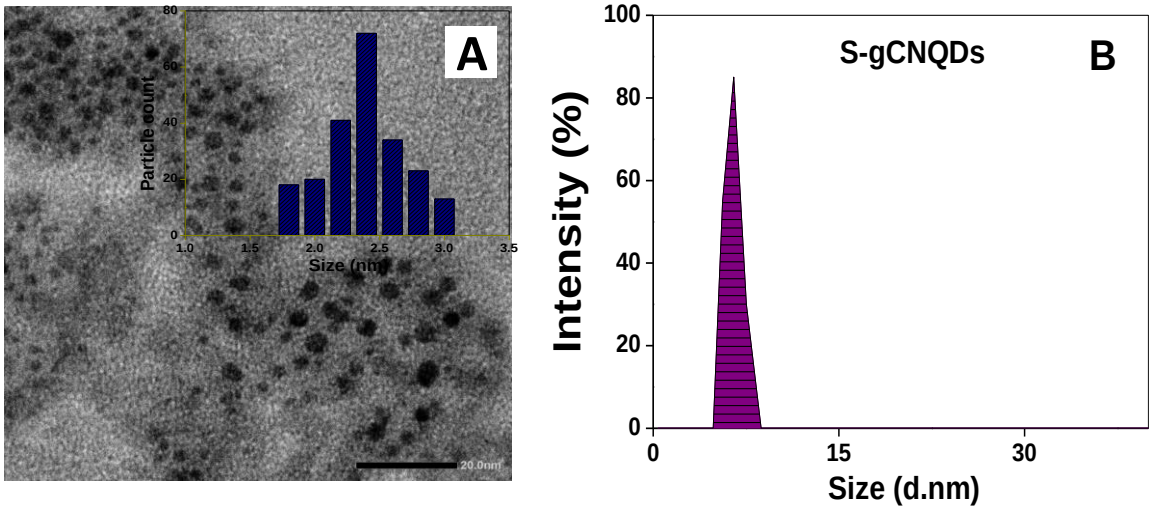

653

654 **Fig. 1.** (A) TEM image of S-gCNQDs (inset is the size distribution histogram). (B)

655 DLS graph of S-gCNQDs.

656

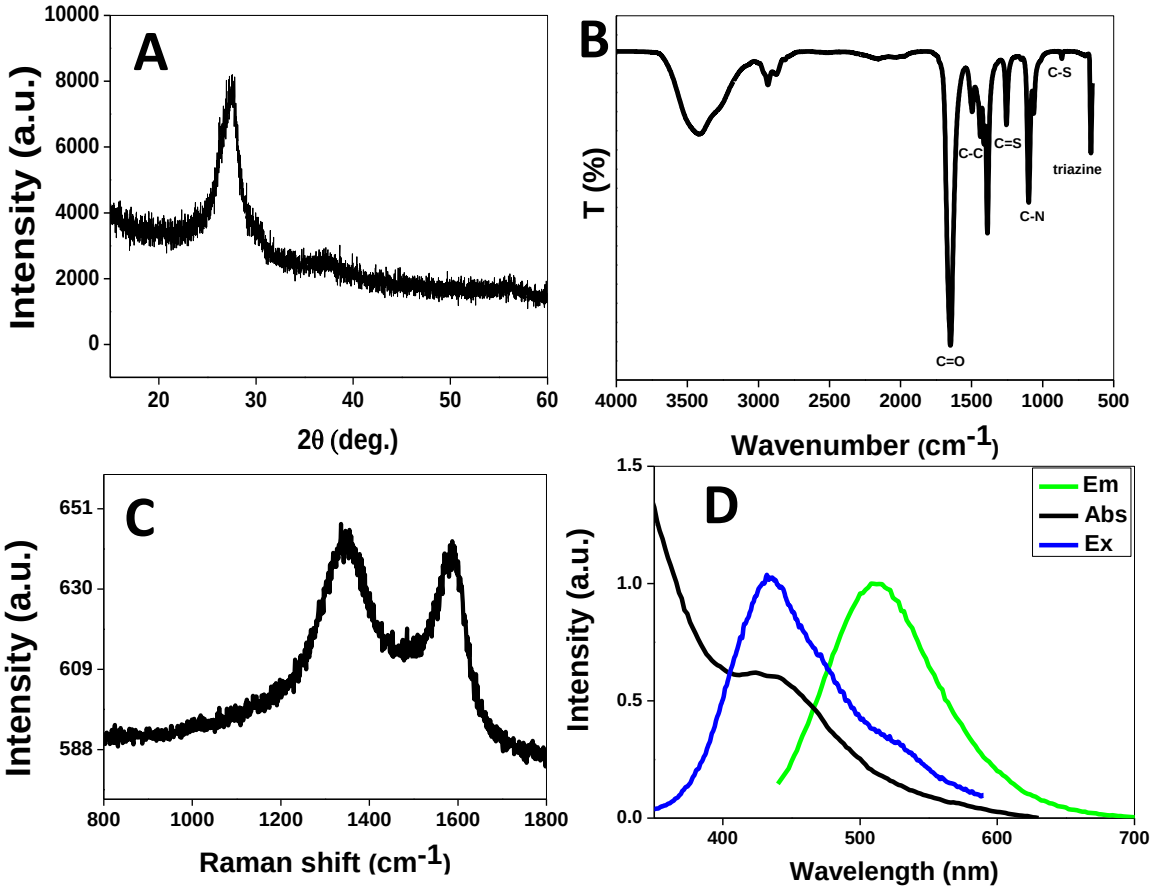

Fig. 2. Characterization spectra of S-gCNQDs showing (A) XRD pattern (B) FTIR absorptions. (C) Raman spectra and (D) UV-vis, excitation, and emission spectra (Solvent – DI water). λ_{ex} = 400 nm.

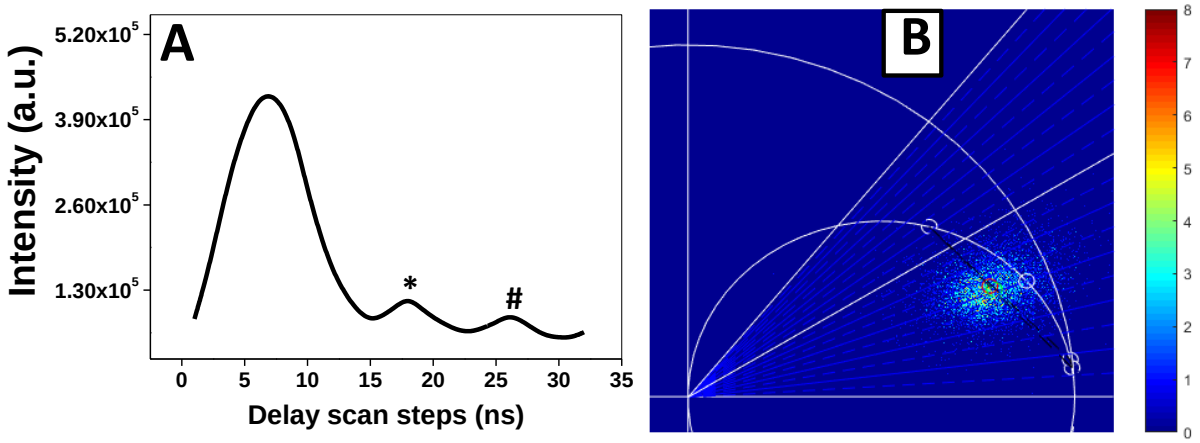

Fig. 3. (A) FL lifetime decay of pristine S-gCNQDs (B) Phasor plot showing the decay component for the analyzing frequency of 20MHz.

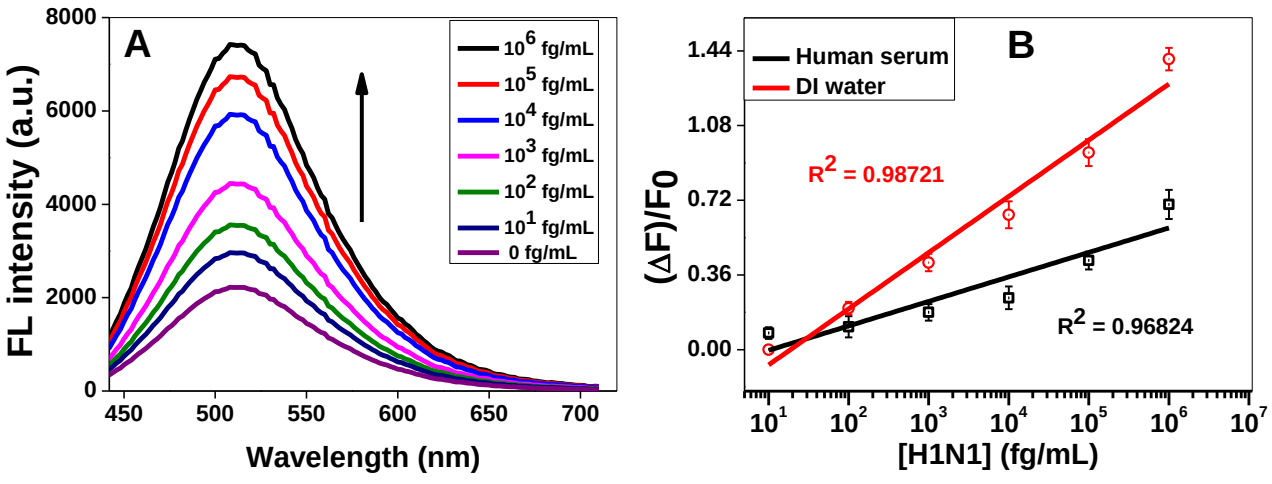

Fig. 4. (A) Detection FL spectra of S-gCNQDs showing enhancement in intensity at various H1N1 virus concentrations. (B) The corresponding calibration plots generated in DI water and human serum. λ_{ex} = 400 nm.

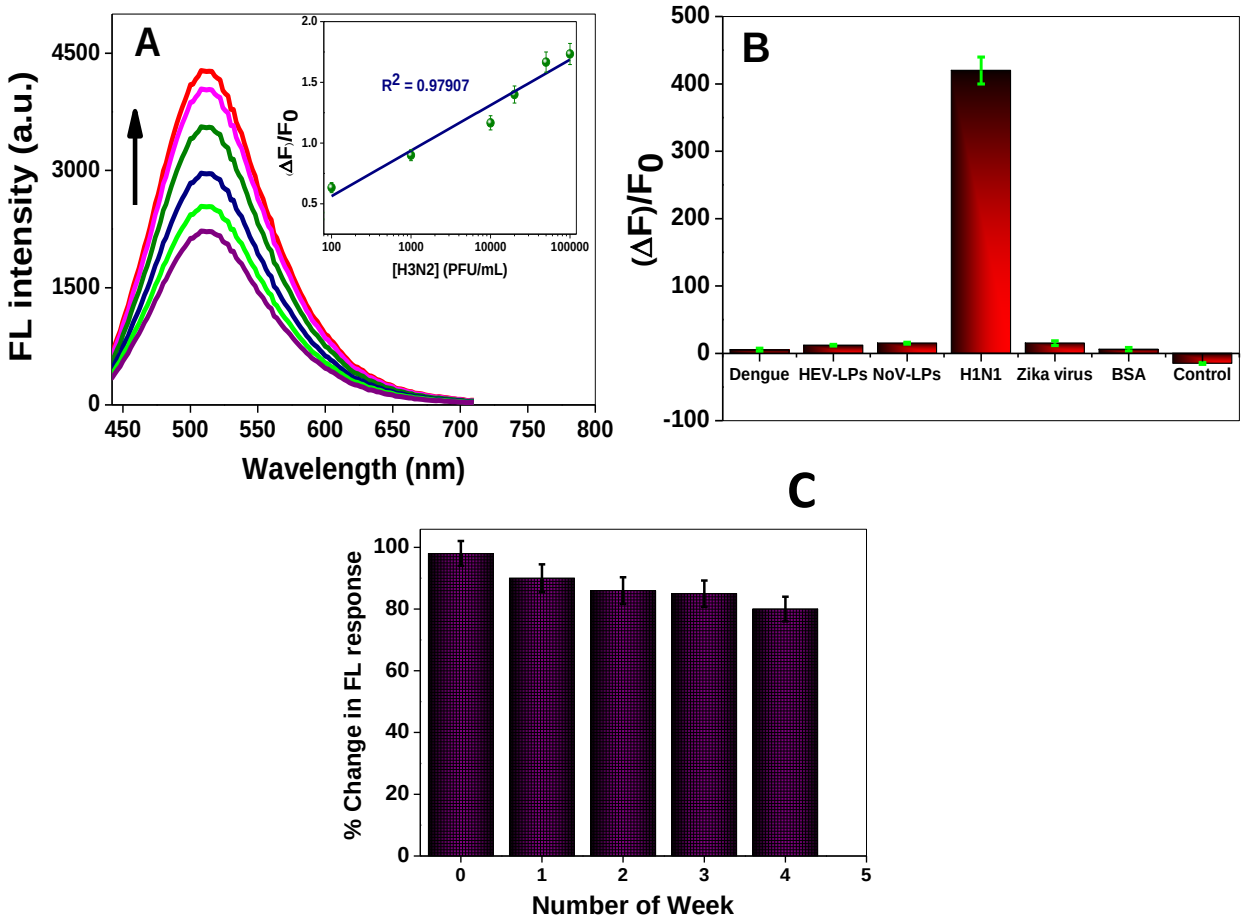

679

680 **Fig. 5.** (A) FL spectra for the detection of clinically isolated influenza A virus
681 (H3N2). Inset: the corresponding calibration plot. (B) Plots showing H1N1
682 selective assay in the presence of other viruses/V-LPS. (C) Stability test of S-
683 gCNQDs and Ag_2S NCs with 1 ng/mL of H3N2 virus showing percentage change
684 in FL signal response over 4 weeks. λ_{ex} = 400 nm.

685

686

687

688

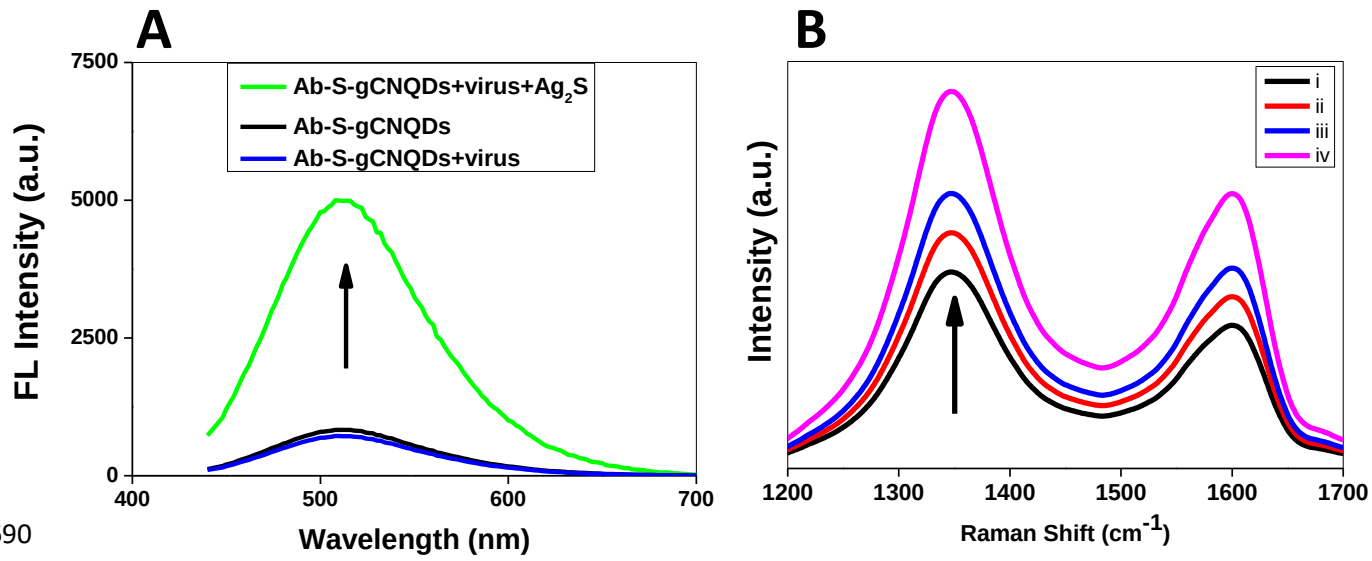

Fig. 6. (A) Fluorescence signal enhancement of S-gCNQDs as in the presence of Ag_2S NCs (B) Corresponding SERS enhancement of S-gCNQDs at different concentrations of Ag_2S NCs due to local optical coupling effects.

Electronic Supplementary Material

Fluoroimmunoassay of influenza virus using sulfur doped-graphitic carbon nitride quantum dots coupled with Ag_2S nanocrystals

Ojodomo J. Achadu[a], De Xing Lioe[b], Keiichiro Kagawa[b], Shoji Kawahito[b], Enoch Y. Park[a,c,*]

[a] *Research Institute of Green Science and Technology, Shizuoka University, 836 Ohya Suruga-ku, Shizuoka 422-8529, Japan*

[b] *Research Institute of Electronics, Shizuoka University, 3-5-1 Johoku, Nakaku, Hamamatsu, Shizuoka 432-8011, Japan*

[c] *Laboratory of Biotechnology, Department of Bioscience, Graduate School of Science and Technology, Shizuoka University, 836 Ohya Suruga-ku, Shizuoka 422-8529, Japan*E-mail:

ojodomo.john.achadu@shizuoka.ac.jp (OJA)
lioe@idl.rie.shizuoka.ac.jp (D.X.L.)
kagawa@idl.rie.shizuoka.ac.jp (K.K.)
kawahito@idl.rie.shizuoka.ac.jp (S.K)
park.enoch@shizuoka.ac.jp (EYP)

[*] Corresponding author: Research Institute of Green Science and Technology, Shizuoka University, 836 Ohya, Suruga-ku, Shizuoka 422-8529, Japan.
E-mail address: park.enoch@shizuoka.ac.jp (E.Y. Park). Tel (Fax): +81-54-238-4887

Synthesis of carboxylic acid-terminated Ag_2S nanocrystals (NCs)

Water-soluble Ag_2S NCs were synthesized following reported procedures with some modifications [1]. In a typical procedure, 0.01 g of $AgNO_3$ salt, 1.2 mL of 3-mercaptopropionic acid and 10 mL of diethylene glycol (DEG) as the reaction solvent, were mixed together and heated up to 120 °C under stirring to form a cloudy mixture. The temperature was further increased to 145 °C for 10 min and the reaction mixture was darkened. The temperature was lowered and the resulting product was allowed to cool to room temperature. Ethanol (95%) was added to the crude product and solid Ag_2S was collected by centrifugation. The product was purified by centrifugation using a mixture of ethanol and acetone to obtain purified Ag_2S NCs. The collected solid product was redispersed in water and stored in the refrigerator for further use.

Characterization Ag_2S nanocrystals

It is imperative to point out here that the use of 3-MPA was for capping and stabilization of Ag_2S NCs, and to provide water-solubility with the rich carboxylic groups of 3-MPA. Thus, morphological characterization using X-ray diffraction analysis was carried out for the prepared Ag_2S NCs. The result verified that the Ag_2S NCs are crystalline, **Fig. S1A** of ESM. The peaks of diffraction in the XRD pattern are very close to those of the monoclinic Ag_2S library pattern (JCPDS Card No. 14-0072) [1]. The TEM image of the prepared Ag_2S NCs revealed particles

which appeared to be separated with non-uniform overall dimension and average size of ~2.5 ± 1.1 nm (**Fig. S1B**). The surface carboxylic acid/sulfide functionalizations were confirmed using FTIR (**Fig. S1C**). Asymmetric and symmetric stretching vibrations are observed for 3-MPA moiety on the Ag_2S NCs. The C–H vibrations of 3-MPA are centered at 2978 cm^{-1} and 2894 cm^{-1}. The -COOH group stretching mode appeared as a prominent peak at 1725 cm^{-1} which is similar to what was observed previously [17]. The characteristic free thiol (SH) absorption (in the MPA) was not observed and this shows that the 3-MPA was bound by the Ag-S binding affinity to the surface of the nanocrystals, which show that the surface of the Ag_2S NCs possesses carboxylic acid terminals due to the use of 3-MPA for capping. The UV-vis absorption spectrum of the Ag_2S NCs displayed absorption band than spans the UV to the visible region, **Fig. S1D**. An intense absorption can be observed at 400 nm which is attributed to the presence of both direct and indirect band gaps in the Ag_2S NCs [1, 2]. In Fig S1E, the overlap of the absorption spectra of Ag_2S NCs and the excitation spectra of S-gCNQDs is shown to reflect the possibility of optoelectronic coupling of the nanoparticles.

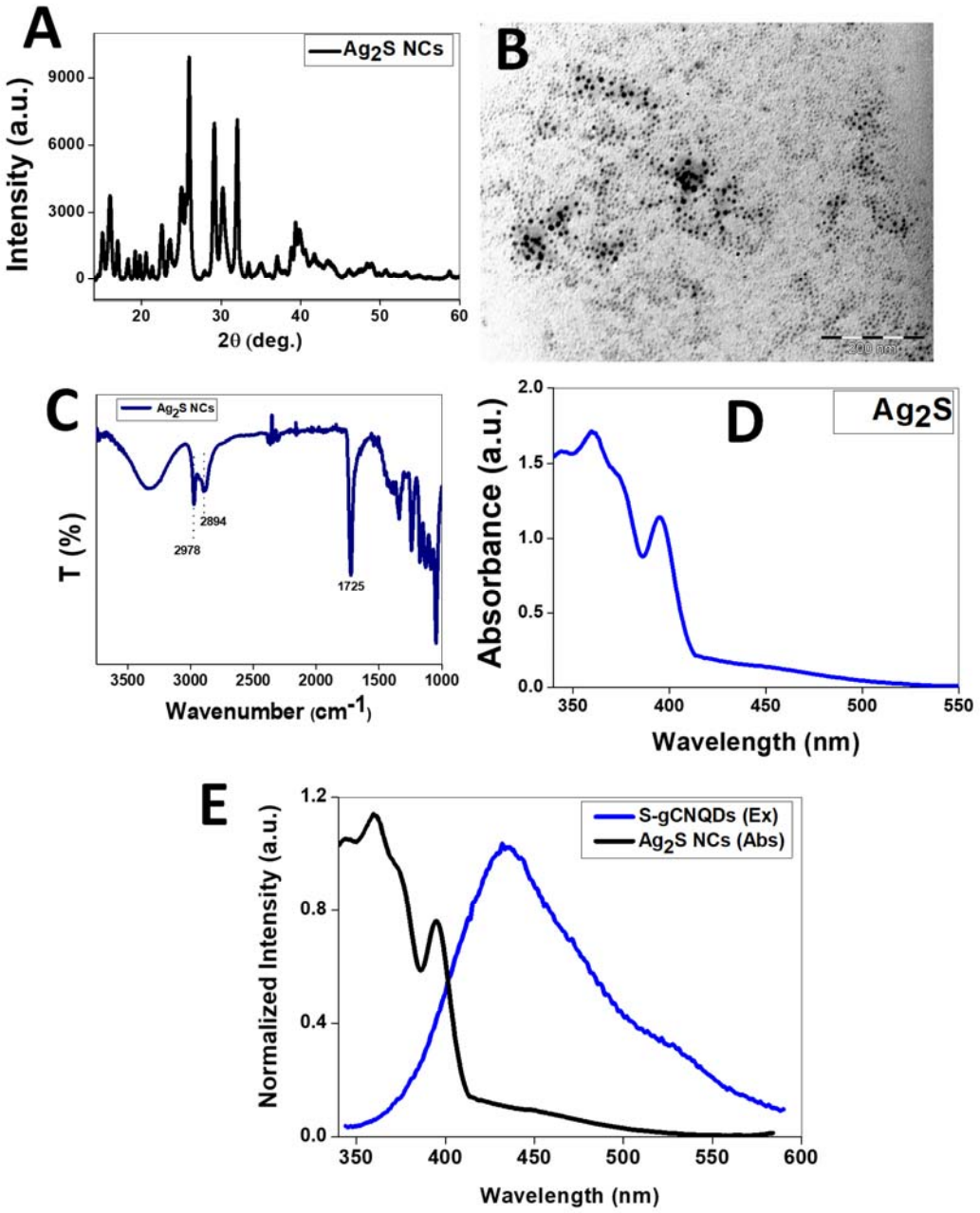

Fig. S1. Characterization results of Ag_2S nanocrystals showing (**A**) Powder XRD pattern (**B**) TEM image (**C**) FTIR spectra and (**D**) Ground state UV-vis absorption spectra. (**E**) Overlap of the absorption spectra of Ag_2S NCs and the excitation spectra of S-gCNQDs.

Optimization and control studies for the developed immunoassay

The immunoassay experiments were characterized with a series of optimization studies before the generation of calibration plots for optimized sensitivity results. The preliminary optimization included (a) the concentration of antibody conjugated S-gCNQDs or Ag_2S NCs needed for maximum FL signal; (b) the concentration range of influenza virus that generate maximum FL signal; (c) the incubation/assay duration, and (d) the stability/reproducibility of the detection FL signal of developed system. The following experimental conditions gave optimum performance of the immunoassay detection of influenza virus: (a) 2 mg/mL of Ab-S-gCNQDs and 1 mg/mL of Ab-Ag_2S NCs in PBS (pH 7.6), respectively. (b) Optimal concentration range of influenza virus for the assay was obtained from 10 fg/mL to 10 ng/mL (c) assay duration was 15 min (d) FL detection signals were stable for more than 15 days. These conditions were further deployed for influenza virus detection in clinical samples.

In order to test the contributions of each species in the developed influenza virus immunoassay protocol, control experiments were conducted. BSA was deployed as a negative control in place of the target influenza virus. The effect of BSA as negative control was tested in the presence of the antibody-conjugated S-gCNQDs or Ag_2S NCs to demonstrate the specific affinity of the antibody conjugated S-gCNQDs or Ag_2S NCs to bind to the target virus via antibody-antigen immunoreactions. Another control experiment conducted was to test the interactions between the S-gCNQDs and Ag_2S NCs with/without antibody

conjugation in the presence or absence of the influenza virus. All experiments were carried under similar conditions. The results obtained from all control experiments are represented in Fig. S2A and B. It can be seen from the results that the FL enhancement of S-gCNQDs was only guaranteed in the presence of the target influenza virus only when the S-gCNQDs and Ag_2S NCs are conjugated to anti influenza virus A antibody (Fig. S2i). To test the influence of Ag_2S NCs in the FL enhancement scheme, Ag_2S NCs (without antibody) and antibody-conjugated Ag_2S NCs were tested. Only the antibody modified Ag_2S NCs was involved in the FL enhancement of S-gCNQDs. This is expectedly due to the immunoreactions between the antibody-conjugated nanostructures and the target influenza virus which bring the S-gCNQDs and Ag_2S NCs close enough to trigger a metal-enhanced fluorescence interaction in the S-gCNQDs. This was also confirmed when no obvious FL change was observed when antibody conjugated Ag_2S NCs was interacted with S-gCNQDs alone (without antibody) in the presence of the target influenza virus (Fig. S2Aiii). Further, the use of BSA as a control did not result in any change in the FL intensity of S-gCNQDs (Fig. S2Biii) as compared to when the target virus was employed (Fig. S2Bii). These results are proof of the specific contribution of the deployed species to the feasibility of the target virus immunoassay.

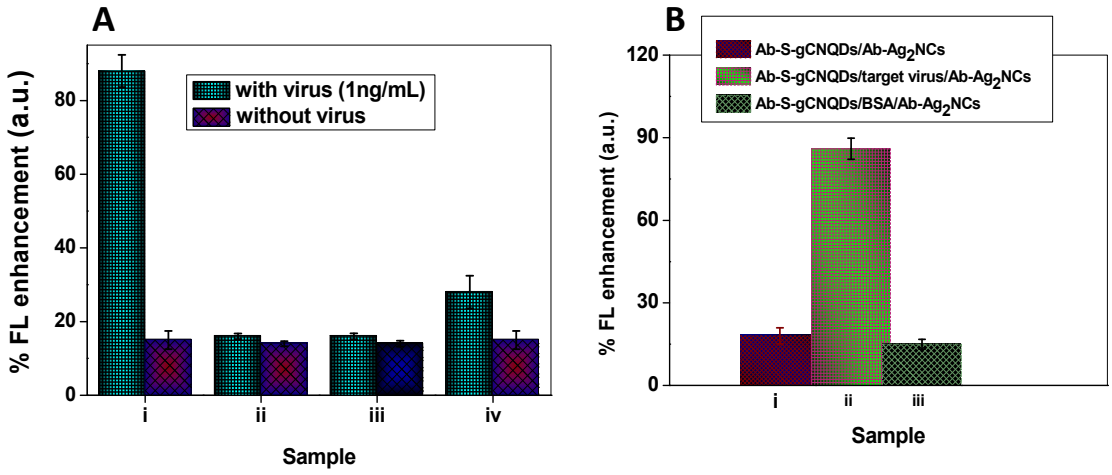

Fig. S2. (**A**) Percent change in FL intensity of (**i**) antibody-S-gCNQDs/antibody-Ag_2S NCs. (**ii**) S-gCNQDs/Ag_2S NCs. (**iii**) S-gCNQDs/antibody-Ag_2S NCs. (**iv**) antibody-S-gCNQDs/Ag_2S NCs. (**B**) the FL response of S-gCNQDs with antibody in the presence of Ag_2S NCS with antibody. (**i**) Without virus. (**ii**) With virus and (**iii**) with BSA.

Fluorescence quantum yield (Φ_F) deteremination

The fluorescence quantum yield of the S-gCNQDs was determined by the comparative method using eqn. 1 [3].

$$\Phi_F = \Phi_{F(Std)} \frac{F.A_{Std}.n^2}{F_{Std}.A.n^2_{Std}} \quad (1)$$

Where A and A_{Std} are the absorbances of the sample and the standard at the excitation wavelength, respectively. F and F_{Std} are the areas under the fluorescence curves of the GQDs and the standard, respectively and n and n_{Std} *are* the refractive indices of the solvent used for the sample and standard, respectively. Rhodamine 6G in ethanol (Φ_F = 0.94 [4]) was used as the standard.

Fluorescence lifetime imaging microscopy (FLIM) experimental setup and Phasor plot generation

The FLIM images were acquired by the FLIM CMOS camera via the Framelink PCIe card (VCE-CLEX02). The CMOS camera has a pixel array of 128 x 128 pixels; each has a four-tap pixel with a pitch of 22.4 μm x 22.4 μm. The sensor response time is 170ps, measured with 472nm laser diode. The Phasor approach was utilized to determine the fluorescence lifetime of the samples [5], instead of the time delay curve method. The graphical view of the Phasor approach simplifies the analysis of the FLIM images. The base frequency for the measurement was 20 MHz, with 32 phase steps. The FPGA in the FLIM CMOS camera scans 32 phases in a period, which was synchronized with the camera exposure operation. The four non-overlap taps of the pixel resulted in four sets of images over 32 phases in one period of scanning. All four sets of images were rearranged and the images from the same phase were summed to increase the signal to noise ratio. The final single set of 32 phases of images was used for the Phasor analysis. Each point in the Phasor plot corresponds to a pixel in the image. The fluorophore/hybrid nanostructure exhibiting a single component will result in the plot on the semicircle. The plot of a multiple-component fluorophore/nanostructure will be situated inside the semicircle. On the semicircle, a very long lifetime corresponds to the Phasor near the origin, while a very short lifetime corresponds to the Phasor at right side of the semicircle.

Fluorescence lifetime imaging microscopy (FLIM) of S-gCNQDs in the presence of target virus

The changes in the lifetime of S-gCNQDs as function of the virus amount were studied using FLIM experiment. The frequency-domain FL lifetimes of S-gCNQDs when conjugated to the antibody and in the virus-induced nanosandwich system was examined. The FL lifetime of S-gCNQDs alone exhibits two-component decay with an average value of 3.19 ns. Meanwhile, in the presence of the H1N1 antibody, the antibody conjugated S-gCNQDs reveals a shortening of their average lifetime to 2.66 ns with a Phasor plot, **Fig. S3B**, indicating a multi-component decay. This indicates an interaction between the S-gCNQDs and the antibody. The S-gCNQDs in the presence of different concentrations of the H1N1 virus at 100 fg/mL, 1.0 pg/mL and 1.0 ng/mL displayed average lifetime values of 4.03, 4.1 and 4.26 ns, respectively (**Fig. S3A, C–E**).

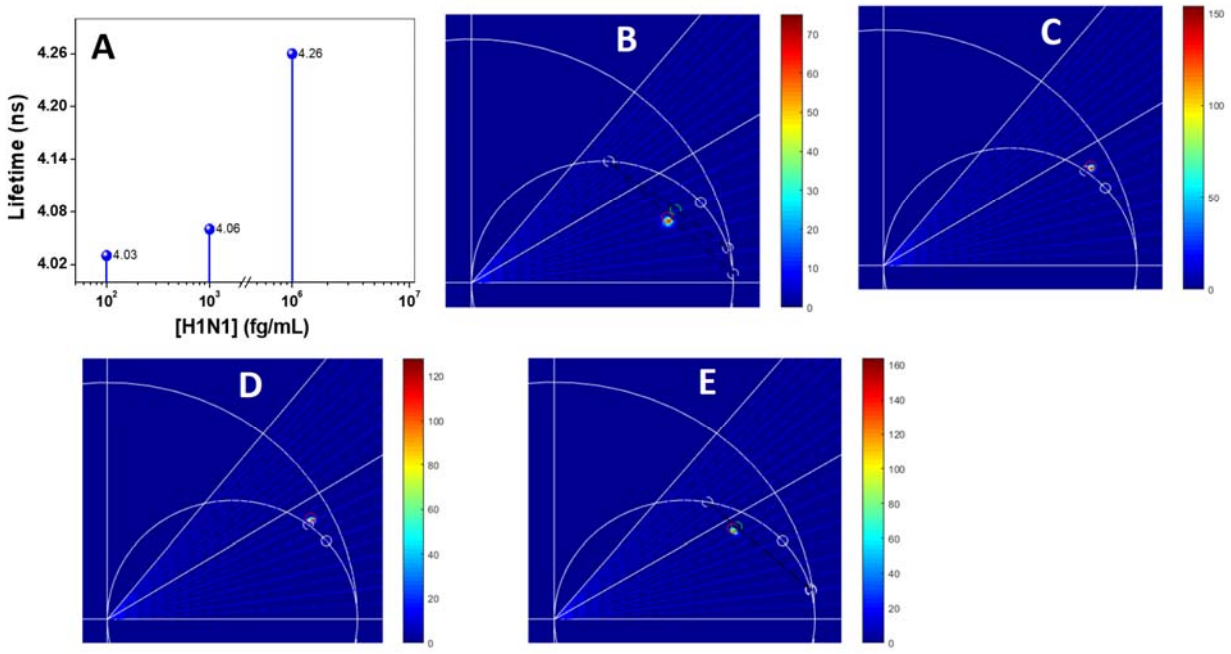

Fig. S3. (A) Changes in fluorescence lifetime of S-gCNQDs as a function of H1N1 virus concentrations. (B–E) Phasor plots for lifetime of S-gCNQDs in the presence (B) Ab (C) 1 ng/mL (D) 1 pg/mL and (E) 1 fg/mL of H1N1 virus.

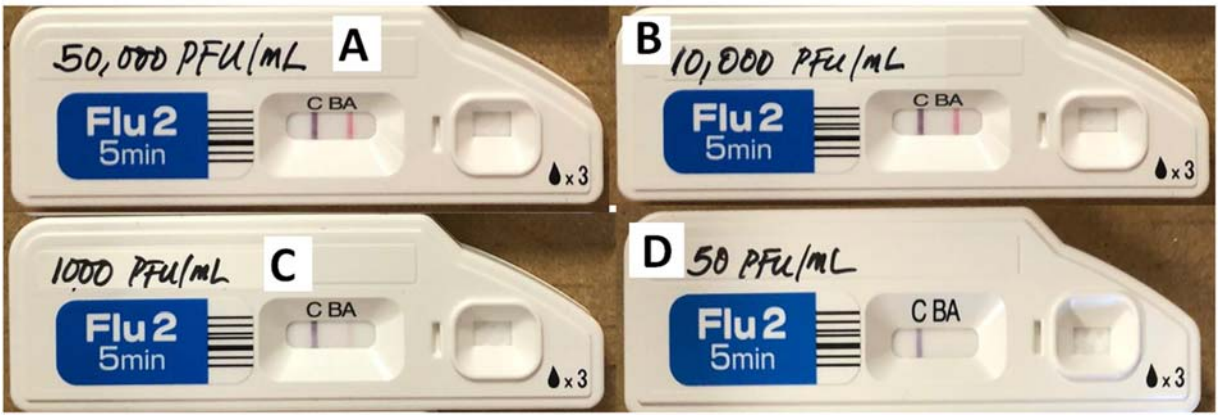

Fig. S4. Commercial RIDT kit for the detection of H3N2 at (A) 50 x 10^3 PFU/mL* (B) 10 x 10^3 PFU/mL* (C) 1 x 10^3 PFU/mL* and (D) 50 PFU/mL. Where A, B, and C denote influenza A virus, influenza B virus, and control, respectively. * Positive result.

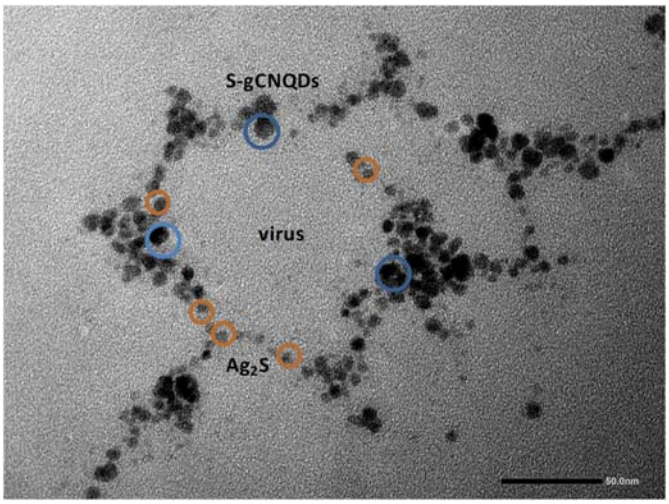

Fig. S5. TEM image of immunocomplex of S-gCNQDs/virus/Ag_2S NCs.

Preparation of sample for surface-enhanced Raman scattering (SERS) measurement

To record the Raman spectra (SERS) of 4-mercaptobenzoic acid (4-MBA) adsorbed on Ag_2S nanocrystals, 10 μL of 4-MBA (1.0×10^{-3} M) in methanol mixed with 20 µL of different concentration of Ag_2S NCs (0.5, 1, 1.5, 2, 2.5 and 3 mg/mL) were dropped onto a silicon substrate, respectively. After air-drying of the solvent, the Raman spectra of the samples were measured. Different laser excitation SERS experiments were conducted using 532 nm laser source. The Raman spectra of S-gCNQDs in the presence of increasing influenza virus concentration and Ag_2S NCs were also measured using the 532 nm laser source.

Demonstration of plasmonic properties of Ag_2S NCs

SERS analysis and results have been used as measure of the plasmonic coupling effects of metallic nanostructures by their ability to enhance the optical Raman scattering signals of a Raman reporter in close proximity. In this work and to demonstrate the plasmonic properties of Ag_2S NCs, SERS analysis was adopted to probe the optical enhancement of the Raman signals of 4-MBA, a classical Raman reporter, in the presence of Ag_2S NCs. As shown in **Fig. S6**, different concentrations of Ag_2S NCs were incubated with 4-MBA and the recorded SERS spectra showed significant increase in the Raman peaks at 1097 and 1596 cm^{-1}, respectively. The Raman signals of 4-MBA were proportionately enhanced with an enhancement factor in the order of 10^5 compared to 4-MBA alone.

In another SERS experiment, the immunocomplexes formed between the antibody-conjugated-S-gCNQDs and antibody-conjugated-Ag_2S NCs incubated with 0.1 and 1 ng/mL of influenza virus were also subjected to Raman measurement to test the SERS enhancement of the S-gCNQDs. In Fig. 6B, the spectra contain the characteristic D band at 1349 cm^{-1} that arises due to the presence of local structural defects known as sp^3 defects. The other peak at 1599 cm^{-1}, called the G-band, a signature of sp^2-containing graphitic structure of S-gCNQDs. The SERS intensity showed appreciable enhancements of the Raman peaks at 1347 and 1599 cm^{-1}, respectively, compared to the antibody-conjugated S-gCNQDs alone (Fig. 6Bi). The SERS analysis results (of S-gCNQDs within the immunocomplex) therefore demonstrates the possibility of metal (plasmonic) coupling effects of Ag_2S NCs as similarly observed for 4-MBA, but with a lower enhancement factor in the order of 10^2. The SERS enhancement of S-gCNQDs within the immunocomplex may have been weakened by the intense fluorescence enhancement of S-gCNQDs in the presence of Ag_2S NCs (Fig. 6A). Meanwhile, no fluorescence signal change or enhancement was observed in the absence of Ag_2S NCs (Fig. 6A) which further confirms the contribution of Ag_2S NCs in the detection process.

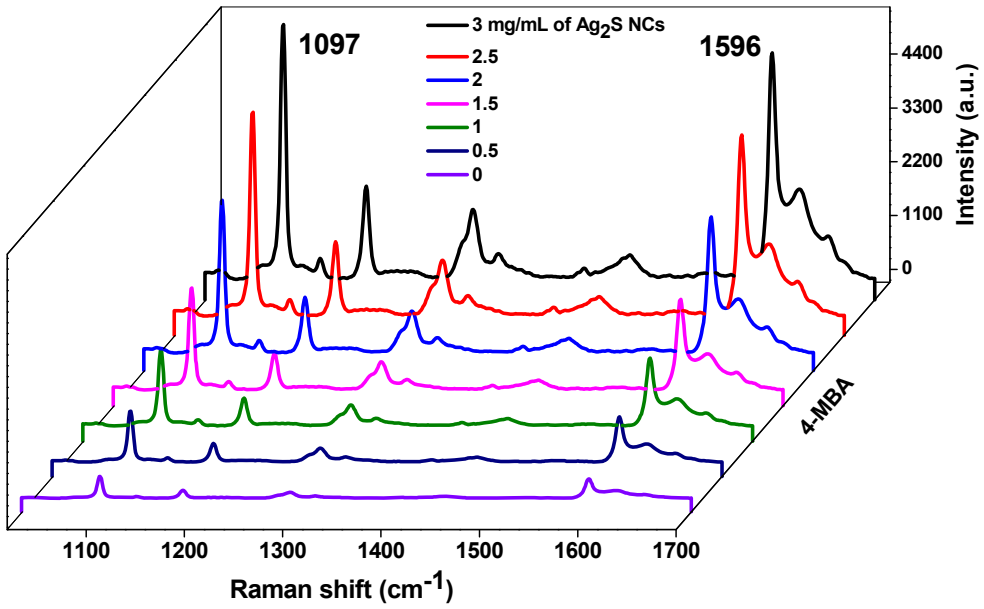

Fig. S6. Raman spectra showing SERS enhancement of 4-MBA in the presence of different concentrations of Ag_2S NCs.

Table S1. A comparison of some recent reports/results on influenza virus detection systems.

Method of detection	Target virus	LOD	Ref.
Fluorescence fiber-optic biosensor	H1N1	13.9 pg/mL	[6]
Magnetofluoro-immunoassay	H1N1	6.07 pg/mL	[7]
Ag-S covalent labelling	H1N1	0.1 pg/mL	[8]
Electrochemical immunosensor	H5N1	2.1 pg/mL	[9]
Metal-enhanced fluoroimmunoassay	H1N1	1 ng/mL	[10]
Peroxidase mimic	H1N1	10 pg/mL	[11]
S-gCNQDs/Ag_2S NCs assay	H1N1	5.5 fg/mL (DI water) and 8.48 fg/mL (in serum)	This work

Table S2. The recovery/immunoassay of clinically isolated influenza A/Yokohama H3N2 virus using the S-gCNQDs probe. (Detection was carried out in human serum).

Sample	Added (PFU/mL)	Found (PFU/mL)	Recovery (%, n = 3)	*RSD (%)
H3N2 Virus	20×10^3	19.5×10^3	97.6±0.15	1.5
	50×10^3	49×10^3	98 ±0.20	2.3
	100×10^3	98×10^3	98 ±0.27	3.1

*Relative standard deviation

References

1. Jiang P, Zhu CN, Zhang ZL, Tian ZQ, Pang DW (2012) Water-soluble Ag_2S quantum dots for near-infrared fluorescence imaging in vivo. Biomaterials 33:5130-5135
2. Li G, Lei Z, Wang QM (2010) Luminescent molecular Ag-S nanoclusters $[Ag_{62}S_{13}(SBu^t)_{32}](BF_4)_4$. J Am Chem Soc. 132:17678-17679
3. Fery-Forgues S, Lavabre D (1999) Are fluorescence quantum yields so tricky to measure? A demonstration using familiar stationery products. J Chem Ed. 76:12660-1264.
4. Fischer S, Georges J (1996) Fluorescence quantum yield of Rhodamine 6G in ethanol as a function of concentration using lens spectrometry. Chemical physics letters. 260:115-118.
5. Seo MW, Shirakawa Y, Kawata Y, Kagawa K, Yasutomi K, Kawahito S (2018) A time-resolved four-tap lock-in pixel CMOS image sensor for real-time fluorescence lifetime imaging icroscopy. IEEE J. Solid-State Circuits. 53:2319–2330
6. Chang, Y.F., Wang, S.F., Huang, J.C., Su, L.C., Yao, L., Li, Y.C., Wu, S.C., Chen, Y.M., Hsieh, J.P., Chou, C., 2010. Biosens. Bioelectron. 26, 1068–1073.
7. Lee, J., Takemura, K., Park, E.Y., 2018. Sens. Actuators, B. 276, 254-261.

8. Li, Y., Hong, M., Qiu, B., Lin, Z., Chen, Y., Cai, Z., Chen, G., 2014. Biosens. Bioelectron. 54, 358-364.
9. U. Jarocka, R. Sawicka, A. Góra-Sochacka, A. Sirko, W. Zagórski-Ostoja, J. Radecki, H. Radecka, Electrochemical immunosensor for detection of antibodies against influenza A virus H5N1 in hen serum, *Biosens. Bioelectron. 55* (2014) 301–306.
10. Ahmed, S.R., Hossain, M.A., Park, J.Y., Kim, S.H., Lee, D., Suzuki, T., Lee, J., Park, E.Y., 2014. Biosens. Bioelectron. 58, 33-39.
11. Ahmed, S.R., Kim, J., Suzuki, T., Lee, J., Park, E.Y., 2016. Biotechnol. Bioeng. 113, 2298-2303.